mutations into hydrophobic amino acids such as tryptophan (W), leucine (L), or methionine (M), or into negatively charged amino acids (including glutamic acid [E]), cause autoactivation (Fig 2, *A* and *B*). The autoactivation was not due to differential protein expression in the transfection assay (see Fig E2 in this article's Online Repository at www.jacionline.org). The R281 and R284 mutations that were assessed remained responsive to cGAMP stimulation (Fig 2, *B* and see Fig E1), indicating no effect on ligand binding. The broad autoactivation of the R281 and R284 mutations was consistent with the model of polymer interface binding to an inhibitor to suppress STING autoactivation.[9] Although this potential inhibitor is not addressed in the 180° rotation model of the connector helix loop mutations, it is quite likely that the 180° rotation also leads to loss of inhibitor binding on the polymer interface, thus allowing side-by-side packing. Our data thus suggest a possible common mechanism to reconcile the 2 previously reported structural models (Fig 2, *C* and see also the Discussion section for detailed description of the model shown in Fig E3 in this article's Online Repository at www.jacionline.org), which is supported by similar superactivating mutations in both the connector helix loop (G158A) and the polymer interface (R281E, R284G, and R284S).

In summary, we have reported 6 patients from 4 unrelated families with recessively inherited *STING1* variants and characteristic clinical features of SAVI. Our data support the notion that the disease-causing homozygous p.R281W variant causes GOF but is weaker in activating STING than the previously reported heterozygous variants, and it requires biallelic mutations to constitutively activate STING. We have demonstrated a critical role of residue R281 in maintaining STING in an inactive state, likely without affecting dimer conformation. Our data unveil limitations of the current structural models that cannot explain the superactivating potential of the R281 and R284 mutations and raise questions as to whether class 3 residues represent an autoinhibitory domain or a binding site for an external inhibitor of STING. Considering the critical function of R281 and the nearby region, novel therapeutic options may arise from high-throughput screens of drugs that bind to this area and inhibit polymerization.

We thank the patients and their families for participating in this study.

*Bin Lin, PhD*[a]*
*Roberta Berard, MD, MSc*[b]*
*Abdulrahman Al Rasheed, MD, MBBS, CAPB*[c]*
*Buthaina Aladba, MD, MBBS, CAPB*[d]*
*Philip J. Kranzusch, PhD*[e,f]
*Maggie Henderlight, BS*[g]
*Alexi Grom, MD*[g]
*Dana Kahle, BS*[a]
*Sofia Torreggiani, MD*[a]
*Alexander G. Aue*[a]
*Jacob Mitchell, BS*[a]
*Adriana A. de Jesus, MD, PhD*[a]
*Grant S. Schulert, MD, PhD*[g]‡
*Raphaela Goldbach-Mansky, MD, MHS*[a]‡

From [a]the Translational Autoinflammatory Diseases Section, Laboratory of Clinical Immunology and Microbiology, National Institute of Allergy and Infectious Diseases, Bethesda, Md; [b]the Department of Pediatrics, Western University, London, Ontario, Canada; [c]the Division of Rheumatology, Pediatric Department, King Abdullah Specialized Children Hospital, King Abdulaziz Medical City, Riyadh, Saudi Arabia; [d]the Sidra Medical and Research Center, Department of Pediatric Medicine, Division of Rheumatology, Doha, Qatar; [e]the Department of Microbiology, Harvard Medical School, Boston, Mass; [f]the Department of Cancer Immunology & Virology, Dana-Farber Cancer Institute, Boston, Mass; and [g]the Cincinnati Children's Hospital Medical Center and Department of Pediatrics, University of Cincinnati College of Medicine, Cincinnati, Ohio. E-mail: goldbacr@mail.nih.gov.

*These authors share co-first authorship.

‡These authors contributed equally to this work.

This research was supported by the Intramural Research Program of the National Institutes of Health (NIH), National Institute of Allergy and Infectious Diseases (to R.G.-M.); grant K08 AR072075 (to G.S.S.) from NIH, National Institute of Arthritis, Musculoskeletal and Skin Diseases; and an Academic Research and Clinical (ARC) grant from Cincinnati Children's Research Foundation (to A.G. and G.S.S.).

Disclosure of potential conflict of interest: R. Goldbach-Mansky has received grant support from SOBI, Regeneron, Novartis, and Eli Lilly. The rest of the authors declare that they have no relevant conflicts of interest.

## REFERENCES

1. Ishikawa H, Ma Z, Barber GN. STING regulates intracellular DNA-mediated, type I interferon-dependent innate immunity. Nature 2009;461:788-92.
2. Ablasser A, Chen ZJ. cGAS in action: Expanding roles in immunity and inflammation. Science 2019;363.
3. Liu Y, Jesus AA, Marrero B, Yang D, Ramsey SE, Sanchez GAM, et al. Activated STING in a vascular and pulmonary syndrome. N Engl J Med 2014;371:507-18.
4. Jeremiah N, Neven B, Gentili M, Callebaut I, Maschalidi S, Stolzenberg MC, et al. Inherited STING-activating mutation underlies a familial inflammatory syndrome with lupus-like manifestations. J Clin Invest 2014;124:5516-20.
5. Melki I, Rose Y, Uggenti C, Van Eyck L, Fremond ML, Kitabayashi N, et al. Disease-associated mutations identify a novel region in human STING necessary for the control of type I interferon signaling. J Allergy Clin Immunol 2017;140:543-52.e5.
6. Kim H, de Jesus AA, Brooks SR, Liu Y, Huang Y, VanTries R, et al. Development of a validated interferon score using nanostring technology. J Interferon Cytokine Res 2018;38:171-85.
7. Shang G, Zhang C, Chen ZJ, Bai XC, Zhang X. Cryo-EM structures of STING reveal its mechanism of activation by cyclic GMP-AMP. Nature 2019;567:389-93.
8. Konno H, Chinn IK, Hong D, Orange JS, Lupski JR, Mendoza A, et al. Pro-inflammation associated with a gain-of-function mutation (R284S) in the innate immune sensor STING. Cell Rep 2018;23:1112-23.
9. Ergun SL, Fernandez D, Weiss TM, Li L. STING polymer structure reveals mechanisms for activation, hyperactivation, and inhibition. Cell 2019;178:290-301.e10.

Available online July 13, 2020.
https://doi.org/10.1016/j.jaci.2020.06.032

## A rare case of selective Igκ chain deficiency: Biologic and clinical implications

*To the Editor:*

Selective Igκ and Igλ deficiencies are extremely rare. So far, there have been few reported cases of Igκ deficiency in the English literature, and all but 2 of them are partial in nature.[1-3] The first reported case of complete Igκ deficiency was that of a male patient with concurrent cystic fibrosis, diabetes mellitus, malabsorption, and IgA deficiency[4]; notably, 1 of the patient's sisters had only trace amounts of $\kappa^+$ immunoglobulins. Sequencing of the κ constant region (*IGKC*) in this patient identified a different single-point mutation in each allele, p.Trp41Arg and p.Cys87Gly, each of which would disrupt stable κ chain folding.[5] The second published case was that of a 62-year-old female from southern Italy who had a history of recurrent respiratory infections and intestinal disorders from early childhood and was homozygous for the p.Cys87Gly point mutation observed in the original patient.[6]

Our patient is a 73-year-old white female; she is a retired nurse who has peripheral neuropathy but is otherwise healthy and with no history of immunodeficiency; nor is there any recorded history

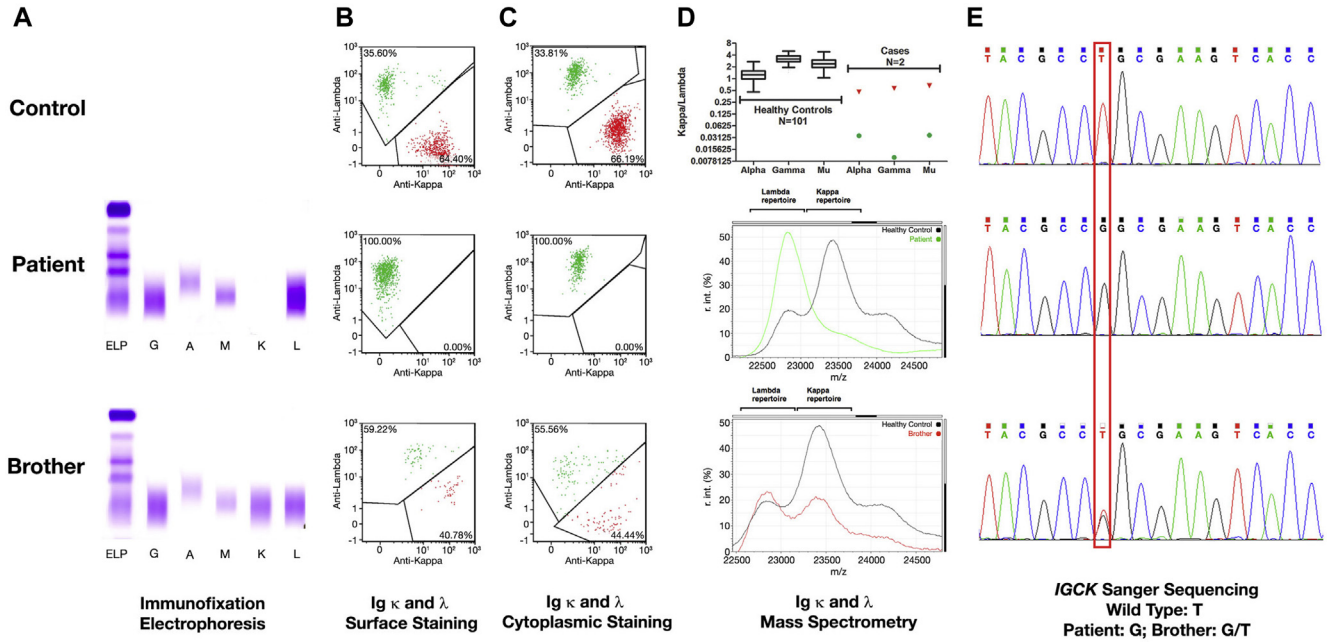


**FIG 1.** Immunofixation electrophoresis showing the complete absence of Igκ in the patient's serum (**A** [*middle panel*]) but its presence in her brother (**A** [*lower panel*]). Flow cytometric analysis indicating the absence of Igκ expression on the surface of the patient's B lymphocytes (**B** [*middle panel*]) and in her B lymphocytes' cytoplasm (**C** [*middle panel*]), in contrast to its expression on the brother's B lymphocytes (**B** [*lower panel*]), and in his B lymphocytes' cytoplasm (**C** [*lower panel*]), but with skewing toward Igλ. Mass spectrometric analysis showing a light chain repertoire consisting entirely of Igλ in the patient (**D** [*middle panel, with green line indicating the patient and black line indicating a healthy control*]), and skewed toward Igλ in her brother (**D** [*lower panel, with red line indicating the patient's brother and black line indicating a healthy control*]); both siblings fall outside the calculated reference interval for the κ/λ heavy chain–to–light chain ratios (**D** [*upper panel, with green symbols indicating the patient and red symbols indicating her brother*]). Sequencing of the κ constant region (*IGKC*) showed a homozygous missense mutation in the patient (**E** [*middle panel*]), whereas the brother is heterozygous (**E** [*lower panel*]).

of autoimmune disease in either the patient or her family. Immunofixation electrophoresis of her serum, which was ordered as part of the assessment for her neuropathy, showed the total absence of Igκ (Fig 1, *A* [*middle panel*]). Mass spectrometric analysis confirmed this finding and the polyclonal nature of the Igλ repertoire (Fig 1, *D* [*middle panel*]). Flow cytometric analysis showed no expression of Igκ in the cytoplasm or on the surface of her B lymphocytes (Fig 1, *B* and *C* [*middle panels*]). B-cell subset immunophenotyping showed a mild decrease in the absolute count of her switched memory B lymphocytes; however, the relative distribution of all subsets within the B-cell compartment was within normal limits (see the results of the performed immunologic assessments in Tables E1-E3 in this article's Online Repository available at www.jacionline.org). Sequencing of *IGKC* showed that she was apparently homozygous for a T>G point mutation leading to p.Cys87Gly (Fig 1, *E* [*middle panel*]), which is identical to that reported in both the first[5] and second[6] published cases. This cysteine is involved in forming 1 of the heavy-to-light interchain disulfide bridges; its mutation interferes with the κ chain's folding.

Our patient has 2 brothers, 1 of whom (a 72-year-old) consented to participate in our study. He had no history of immunodeficiency and showed moderate B-cell lymphopenia, a mild decrease in the percentage of plasmablasts, a skewed κ/λ ratio in the serum (Fig 1, *D* [*lower panel*]), and decreased κ/λ expression in the cytoplasm and on the surface of his B lymphocytes (Fig 1, *B* and *C* [*lower panels*]) but was otherwise normal. Sequencing of his *IGKC* demonstrated that he was heterozygous for p.Cys87Gly (Fig 1, *E* [*lower panel*]), the missense mutation identified in his sister.

On the basis of the total absence of Igκ on immunofixation electrophoresis and before the genetic analysis, the patient's primary physician had referred her to a hematologist who proceeded with ordering a bone marrow aspirate and biopsy. Flow cytometric analysis of the aspirate at a commercial diagnostic service showed a λ-restricted B-lymphocyte population and the absence of $\kappa^+$ B lymphocytes (see Fig E1, *A* in the Online Repository available at www.jacionline.org), which is consistent with our data on the patient's peripheral blood. This prompted cytogenetic/fluorescence in situ hybridization studies, which showed a normal female karyotype and negative fluorescence in situ hybridization probe results for CEP3, MYB, CEP7, CCND1, BCL1/IGH, BIRC3/MALT1, and TP53/CEP17. In addition, the patient's bone marrow was reported to be normocellular with trilineage hematopoiesis and no significant dyspoiesis. Because of the λ-restricted B-lymphocyte population, these findings were collectively misconstrued as minimal bone marrow involvement by a B-cell lymphoproliferative disorder, with lymphoplasmacytic lymphoma and marginal zone lymphoma as the differential diagnoses.

The patient's bone marrow slides were reviewed at Mayo Clinic. The review confirmed the observed normal trilineage hematopoiesis (see Fig E1, *B*), with no conspicuous decrease in

lymphocyte level (see Fig E1, *C*). The immunohistochemistry findings for $CD3^+$ T cells and $CD20^+$ B cells were normal (see Fig E1, *D-G*). On the basis of the bone marrow studies and other acquired data, the presence of lymphoma was ruled out.

To our knowledge, there has been no other case of isolated Igκ absence on immunofixation electrophoresis at Mayo Clinic. This notwithstanding, we compared the Ig heavy chain and light chain mass distributions of the patient and her brother with a reference interval established by using sera from 101 healthy controls. This was achieved by using a peak modeling algorithm to identify and analyze the Ig heavy chain and light chain mass distributions and also to calculate the κ/λ heavy chain–to–light chain ratios. Fig 1, *D* (*top panel*) shows that both the patient (*lower right*) and her brother (*upper right*) clearly fall outside the established reference interval.

These findings provide conclusive evidence for a case of primary Igκ deficiency. They confirm that complete absence of Igκ does not prevent the emergence of $\lambda^+$ B lymphocytes, which is consistent with experimental findings in Cκ-mutant mice,[7] as well as in mice with inactivated Cκ intron enhancer.[8] The originally described patient with complete Igκ deficiency did not show excessive susceptibility to infection.[4] Similarly, despite her career as a health care professional with frequent exposure to patients, our patient had an unremakable history with respect to infection. By contrast, the Italian patient has had a lifelong history of recurrent infections, leading the authors to attribute her infections to Igκ deficiency.[6] On the basis of our findings and the report on the original patient,[4] we call into question this assertion and find it improbable that Igκ deficiency would in itself manifest as a symptomatic immunodeficiency. The experimental models point to a decrease in the total number of B cells in the bone marrow, spleen, and peripheral blood of the mutant mice.[7,8] The normal number of CD19 B cells in our patient's bone marrow sample and her normal peripheral B-cell count, as well as the lack of any gross abnormality in B-cell enumeration in the other patients,[4,6] argue against a similar scenario in humans. In this respect, the B-cell lymphopenia observed in our patient's brother could potentially be due to a decline in B-cell lymphopoiesis with age[9] rather than being a consequence of the heterozygous mutation that he shares with his sister. Additionally, the decrease in the κ/λ ratio in the patient's brother points to the quantitative effect of the defective *IGKC* allele on Igκ expression. This notion is supported by the findings in a patient with *de novo* deletion of (2) (p11.2p13), who showed a decrease in κ/λ ratio when compared with his mother and an unrelated control.[3] The hematopathology report on our patient showed that the complete absence of $\kappa^+$ B lymphocytes can be misconstrued as a clonal B-cell lymphoproliferative disease. Therefore, although complete Igκ deficiency is very rare (an estimated 1 to 2 cases per million),[E5-E8] it should be included in the differential diagnosis of clonal B-cell lymphoproliferative disorders.

We thank Boudinot T. Atterbury, MD, for his care of the patient, and Attila Kumanovics, MD, for his critical reading of this article and his invaluable input.

*Amir A. Sadighi Akha, MD, DPhil*[a]*
*Renee C. Tschumper, BS*[b]
*John R. Mills, PhD*[a]
*Crescent R. Isham, BS*[a]
*Elizabeth E. Witty, MS*[a]
*David S. Viswanatha, MD*[a]
*Surendra Dasari, PhD*[a]
*Melissa R. Snyder, PhD*[a]
*David L. Murray, MD, PhD*[a]
*Jerry A. Katzmann, PhD*[a]
*Diane F. Jelinek, PhD*[b]
*Maria A. V. Willrich, PhD*[a]*

From [a]the Department of Laboratory Medicine and Pathology and [b]the Department of Immunology, Mayo Clinic, Rochester, Minn. E-mail: sadighiakha.amir@mayo.edu. Or: willrich.mariaalice@mayo.edu.

*These authors contributed equally to this work.

Disclosure of potential conflict of interest: D. L. Murray, J. R. Mills, and S. Dasari have intellectual property and receive royalties related to the analysis of immunoglobulins by mass spectrometry. The rest of the authors declare that they have no relevant conflicts of interest.

## REFERENCES

1. Bernier GM, Gunderman JR, Ruymann FB. Kappa-chain deficiency. Blood 1972;40:795-805.
2. Barandun S, Morell A, Skvaril F, Oberdorfer A. Deficiency of kappa- or lambda-type immunoglobulins. Blood 1976;47:79-89.
3. Los FJ, Van Hemel JO, Jacobs HJ, Drop SL, van Dongen JJ. De novo deletion (2)(p11.2p13): clinical, cytogenetic, and immunological data. J Med Genet 1994;31:72-3.
4. Zegers BJ, Maertzdorf WJ, Van Loghem E, Mul NA, Stoop JW, Van Der Laag J, et al. Kappa-chain deficiency. An immunoglobulin disorder. N Engl J Med 1976;294:1026-30.
5. Stavnezer-Nordgren J, Kekish O, Zegers BJ. Molecular defects in a human immunoglobulin kappa chain deficiency. Science 1985;230:458-61.
6. Sala P, Colatutto A, Fabbro D, Mariuzzi L, Marzinotto S, Toffoletto B, et al. Immunoglobulin K light chain deficiency: a rare, but probably underestimated, humoral immune defect. Eur J Med Genet 2016;59:219-22.
7. Zou YR, Takeda S, Rajewsky K. Gene targeting in the Ig kappa locus: efficient generation of lambda chain-expressing B cells, independent of gene rearrangements in Ig kappa. EMBO J 1993;12:811-20.
8. Takeda S, Zou YR, Bluethmann H, Kitamura D, Muller U, Rajewsky K. Deletion of the immunoglobulin kappa chain intron enhancer abolishes kappa chain gene rearrangement in cis but not lambda chain gene rearrangement in trans. EMBO J 1993;12:2329-36.
9. Scholz JL, Diaz A, Riley RL, Cancro MP, Frasca D. A comparative review of aging and B cell function in mice and humans. Curr Opin Immunol 2013;25:504-10.

Available online April 8, 2020.
https://doi.org/10.1016/j.jaci.2020.02.023

# The regulatory activity of autophagy in conjunctival fibroblasts and its possible role in vernal keratoconjunctivitis

*To the Editor:*

Vernal keratoconjunctivitis (VKC) is a rare, IgE- and non–IgE-mediated form of ocular allergy affecting children and young adults living in warm climates. It can be severe and can cause permanent visual disabilities because of frequent corneal involvement.[1] Levels of $T_H2$-type cytokines, along with levels of other proinflammatory cytokines, growth factors, and enzymes, are increased in patients with VKC,[2] suggesting that multiple patterns of conjunctival inflammation are involved. TNF-α has been shown to be localized in conjunctival mast cells and increased in tears and in conjunctival tissues of patients with VKC.[3] TNF-α increases the inflammatory cell influx into the conjunctiva by upregulating the expression of adhesion

# METHODS

## Ethics statement

The samples were obtained from the patient and her brother after they had consented to an approved institutional review board protocol at Mayo Clinic.

## Serum protein electrophoresis and immunofixation, immunoglobulin quantitation

Reagents for serum protein electrophoresis (SPEP) were purchased from Helena Laboratories (Beaumont, Tex) and for immunofixation from Sebia (Norcross, Ga). SPEP was performed on the SPIFE 3000 electrophoresis analyzer (Helena Laboratories). Serum immunofixation was performed on Hydrasys 9IF gels (Sebia). Total serum protein concentration was measured by a colorimetric assay with (biuret method) on an Advia 1200 chemistry analyzer (Siemens Healthcare, Marburg, Germany). Nephelometric assays were used to measure total immunoglobulin levels (Siemens), IgG and IgA subclasses, free κ and free λ light chains, and heavy chain–light chain pairs (all from The Binding Site, Birmingham, United Kingdom), on BNII instruments (Siemens). Serum samples were analyzed by using standard operating procedures from the clinical laboratory for all assays.[E1]

## Flow cytometry

T-cell, B-cell, and natural killer cell enumeration was performed by using a single-platform approach, with all antibodies purchased from Beckman Coulter (Miami, Fla). CD45 lymphocytes were defined by side scatter and CD45 (clone J33) gating, followed by exclusion of any remaining cells positive for CD14 (clone RMO52). Within this population, total T cells were identified with CD3 (clone UCHT1), and the T-cell subsets were identified with CD4 (clone 13B8.2) and CD8 (clone B9.11) staining, respectively; B cells were defined by CD19 (clone J3-119) staining, and natural killer cells by CD16 (clone 3G8) and CD56 (clone N901) staining.

Surface and cytoplasmic $Ig\kappa^+$ and $Ig\lambda^+$ B cells were identified as follows: CD45 lymphocytes were defined by side scatter and CD45 (clone 2D1) gating. Afterward, $\kappa^+$ and $\lambda^+$ B cells were identified within the $CD19^+$ (clone SJ25C1) $CD20^+$ (clone L27) $CD5^-$ (clone L17F12) cells. Neither the patient nor her brother or the control had any $CD19^+CD20^+CD5^+$ B cells. The anti-κ and anti-λ antibodies were obtained from Dako North America (Santa Clara, Calif). The rest were acquired from Becton Dickinson (San Jose, Calif).

B-cell subset immunophenotyping was performed by using antibodies against the following: CD45 (clone 2D1), CD19 (clone 4G7), CD20 (clone L27), CD21 (clone B-ly4), CD27 (clone 1A4), CD38 (clone HB7), IgM (clone G20-127), and IgD (clone IA6-2). The anti-CD27 antibody was purchased from Beckman Coulter. The rest were obtained from Becton Dickinson.

CD45 lymphocytes were defined by side scatter and CD45 gating. Within this population, $CD19^+$ and $CD20^+$ B cells were identified by CD19 and CD20 staining, respectively. Within the $CD45^+CD19^+$ cells, B-cell subsets were defined as follows: total memory B cells were determined by using $CD27^+$ staining, nonswitched memory B cells were determined by using $CD27^+IgM^+IgD^+$ staining, switched memory B cells were identified by using $CD27^+IgM^-IgD^-$ staining, transitional B cells were determined by using $CD38^+IgM^+$ staining, plasmablasts were determined by using $CD38^+IgM^-$ staining, and CD21 B cells were determined by using $CD21^+$ staining.

## MALDI-TOF

Matrix-assisted laser desorption ionization–time of flight (MALDI-TOF) instruments for detecting monoclonal proteins have recently been introduced to the clinical laboratory.[E2,E3] The reagents for mass spectrometry included ammonium bicarbonate, dithiothreitol, and formic acid (Sigma-Aldrich Inc, St Louis, Mo). Water, 2-propanol, and acetonitrile were obtained from Honeywell Burdick and Jackson (Muskegon, Mich). The methods combine nanobody immunoenrichment with use of MALDI-TOF mass spectrometry to identify, isotype, and assess the heavy chain–light chain pairings and quantitate M-proteins. Briefly, serum was mixed in 5 different tubes for enrichment. Enrichment was performed by using commercially available camelid-derived nanobodies directed against the heavy chain constant domains of IgG, IgA, and IgM or the light chain constant domains of κ and λ immunoglobulins (Life Technologies). Briefly, 10 μL of beads was incubated with 20 μL of serum diluted into 180 μL of PBS for at least 30 minutes at room temperature. Subsequently, the supernatant was removed and the beads were washed 3 times with 200 μL of PBS and then twice with 200 μL of water. Samples were eluted with 80 μL of 5% acetic acid containing 50 mM tris(2-carboxyethyl)phosphine. Subsequently, 0.6 μL of each eluent was spotted onto a single well of a 96-well microScout polished steel Bruker target plate (Bruker Daltonics, Billerica, Mass) prespotted with matrix (α-cyano-4-hydroxycinnamic acid, 10 mg/mL in 50% acetonitrile plus 0.1% trifluoroacetic acid). After sample addition, 0.6 μL of matrix was layered on top of each sample. Mass analysis was performed in a positive ion mode with summation of 500 laser shots using a MALDI-TOF mass spectrometer (Bruker Microflex LT). Spectra were generated corresponding to a mass range of 9,000 to 32,000 m/z.

The polyclonal light chains are distributed in multiple charge states (+2 and +1). These appear as overlapping gaussian distributions corresponding to the λ and κ light chains. Polyclonal light chains are identified in the mass spectra of proteins enriched by light chain–specific nanobodies as well as in the mass spectra of proteins enriched by heavy chain–specific nanobodies. A peak modeling algorithm was developed to interpret each of the mass spectra. With use of this algorithm, immunoglobulin heavy chain and light chain mass distributions were identified and analyzed. Furthermore, the κ/λ heavy chain–to–light chain ratios were calculated. Reference intervals were established by using residual waste sera from a cohort of 101 healthy controls with a negative SPEP result, negative immunofixation result, and negative free light chain assay result obtained from the Protein Immunology Laboratory at Mayo Clinic. In contrast to the mass spectra in the healthy adult population, samples with M-proteins have nongaussian distributions of both light and heavy chain masses, with narrower widths and shifted apexes (both in mass-to-charge ratios) that are restricted to mass spectra corresponding to the isotype of the M-protein when compared with samples from the reference population.

## PCR amplification and sequencing

PBMCs from patients were isolated by Ficoll-Paque (GE Healthcare, Piscataway, NJ) density centrifugation. B cells were purified by using the StemCell B-Cell Enrichment kit and a Robosep instrument (StemCell Technologies, Vancouver, British Columbia, Canada). RNA was isolated from half of the cells by using the Trizol method (Life Technologies, Carlsbad, Calif), with1 μg converted to cDNA by using the iScript cDNA Synthesis kit (Bio-Rad, Hercules, Calif). DNA was isolated from the remaining cells by using the ArchivePure DNA isolation kit (5 Prime, Inc, Gaithersburg, Md). cDNA and DNA from non-B cells were also included in the PCR. Amplification for the κ constant region was carried out by using 2 μL of cDNA or 200 ng of DNA with the HotStarTaq MasterMix (Qiagen, Valencia, Calif) under the following conditions: denaturation at 95°C for 15 minutes; 35 cycles of 95°C for 30 seconds, 60°C for 60 seconds, and 72°C for 60 seconds, with a final extension of 72°C for 10 minutes. A β-actin reaction was included for each template. Amplified products were electrophoresed on a 1.5% agarose– Tris-acetate-EDTA gel and visualized with ethidium bromide. Bands were excised, purified with a Promega Wizard PCR Prep kit (Madison, Wis), and sequenced in both the 5′ and 3′ directions by using the same primers used for amplification. To further verify the sequence, the PCR products were subcloned into a TOPO TA vector (Invitrogen/Thermo Fisher, Waltham, Mass) and colonies were grown, prepped (QIAprep Spin Miniprep kit, Qiagen), and sequenced by using vector primers in both the 5′ and 3′ directions.

Direct sequencing of the amplified products and subsequent subclones from the patient revealed a consistent point mutation from thymine to guanine, resulting in an amino acid change from cysteine to glycine at amino acid position 87; as a matter of consistency, all amino acid positions in the text are based on the International Immunogenetics nomenclature.[E4] Sequencing of control normal B-cell products showed a wild-type sequence at this location. Direct sequencing of the amplified product from the patient's brother showed a heterozygous phenotype at the same nucleotide position. When the amplified

products were subcloned, the sequences were nearly half thymine and half guanine, indicating that 1 allele was affected whereas the other remained wild type.

The study of variation across 141,456 human exomes and genomes[E5] puts the frequency of homozyosity for the cysteine-to-glycine mutation at approximately 1.5 per million in Europeans but lower for other evaluated populations.[E6] This, together with the estimated frequency of other evaluated loss-of-function *IGKC* variants,[E7,E8] puts the aggregate estimate for Igκ deficiency at 1 to 2 per million.

## REFERENCES

E1. Katzmann JA, Kyle RA, Benson J, Larson DR, Snyder MR, Lust JA, et al. Screening panels for detection of monoclonal gammopathies. Clin Chem 2009; 55:1517-22.

E2. Mills JR, Kohlhagen MC, Dasari S, Vanderboom PM, Kyle RA, Katzmann JA, et al. Comprehensive assessment of M-proteins using nanobody enrichment coupled to MALDI-TOF mass spectrometry. Clin Chem 2016;62:1334-44.

E3. Kohlhagen MC, Barnidge DR, Mills JR, Stoner J, Gurtner KM, Liptac AM, et al. Screening method for M-proteins in serum using nanobody enrichment Coupled to MALDI-TOF mass spectrometry. Clin Chem 2016;62:1345-52.

E4. Lefranc MP, Giudicelli V, Duroux P, Jabado-Michaloud J, Folch G, Aouinti S, et al. IMGT(R), the international ImMunoGeneTics information system(R) 25 years on. Nucleic Acids Res 2015;43:D413-22.

E5. Karczewski KJ, Francioli LC, Tiao G, Cummings BB, Alföldi J, Wang Q, et al. Variation across 141,456 human exomes and genomes reveals the spectrum of loss-of-function intolerance across human protein-coding genes. bioRxiv preprint 2019 posted August 13, 2019. Available at: https://doi.org/10.1101/531210.

E6. gnomADbrowser. Single nucleotide variant: 2-89156939-A-C (GRCh37). Available at: https://gnomad.broadinstitute.org/variant/2-89156939-A-C?dataset=gnomad_r2_1. Accessed December 7, 2019.

E7. gnomADbrowser. IGKC immunoglobulin kappa constant. Available at: https://gnomad.broadinstitute.org/gene/ENSG00000211592?dataset=gnomad_r2_1. Accessed December 7, 2019.

E8. gnomADbrowser. Deletion: 89157033-ACT-A (GRCh37). Available at: https://gnomad.broadinstitute.org/variant/2-89157033-ACT-A?dataset=gnomad_r2_1. Accessed December 7, 2019.

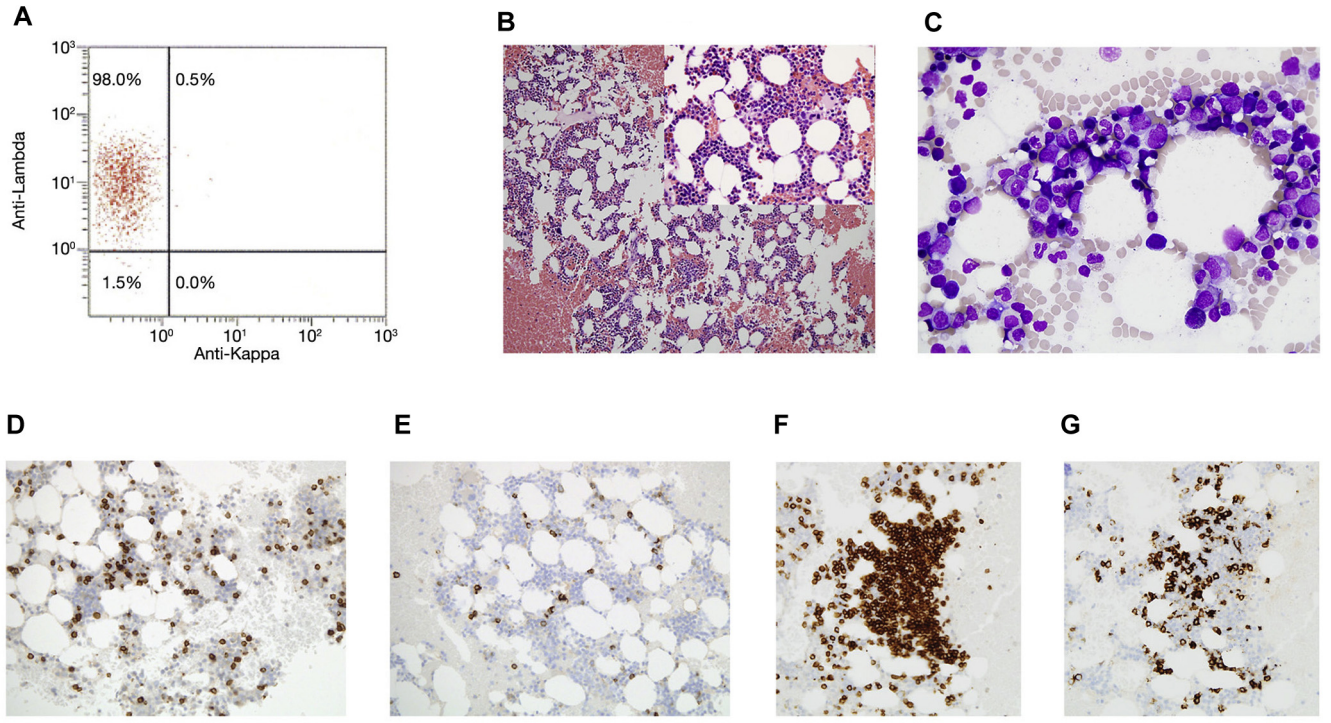


**FIG E1.** Flow cytometric assessment of the patient's bone marrow showing the absence of $\kappa^+$ B lymphocytes **(A)**. The patient has morphologically normal trilineage hematopoiesis (hematoxylin and eosin stain at medium magnification with inset at ×40 magnification **[B];** Wright-Giemsa stain at ×40 magnification **[C]**). Normal findings by immunohistochemistry for $CD3^+$ T cells **(D)** and $CD19^+$ B cells **(E)**. Small lymphoid nodule with benign morphologic features consisting predominantly of $CD3^+$ T cells **(F)** and including a few small $CD19^+$ B cells **(G)**.

**TABLE E1.** Serum protein electrophoresis, immunofixation, and total immunoglobulin and free light chain quantitation results in the patient and her brother

| Assay | Reference interval | Patient | Brother |
|---|---|---|---|
| Total protein | 6.3-7.9 g/dL | 8.0 | 7.0 |
| Albumin | 3.4-4.7 g/dL | 4.2 | 3.6 |
| Alpha 1 | 0.1-0.3 g/dL | 0.3 | 0.2 |
| Alpha 2 | 0.6-1.0 g/dL | 0.9 | 0.9 |
| Beta | 0.7-1.2 g/dL | 1.2 | 0.8 |
| Gamma | 0.6-1.6 g/dL | 1.4 | 1.5 |
| Immunofixation | | No monoclonal protein detected | No monoclonal protein detected |
| Total IgG | 767-1590 mg/dL | 1009 | 960 |
| IgG1 | 341-894 mg/dL | 524 | 404 |
| IgG2 | 171-632 mg/dL | 339 | 495 |
| IgG3 | 18.4-106 mg/dL | 73.3 | 91.6 |
| IgG4 | 2.4-121 mg/dL | 24.4 | 12.4 |
| Total IgA | 61-356 mg/dL | 175 | 179 |
| IgA1 | 50-314 mg/dL | 131 | 135 |
| IgA2 | 9.7-156 mg/dL | 22 | 27.6 |
| Total IgM | 37-286 mg/dL | 335 | 246 |
| Total IgD | <10 mg/dL | <0.68 | <0.61 |
| Free κ | 0.33-1.94 mg/dL | <0.0276 | 2.21 |
| Free λ | 0.57-2.63 mg/dL | 2.94 | 2.16 |
| κ/λ ratio | 0.26-1.65 | 0.0374 | 1.02 |

**TABLE E2.** T-cell, B-cell, and natural killer cell enumeration results in the patient and her brother

| Cell type | Reference interval | Patient | Brother |
|---|---|---|---|
| CD45 lymphocyte count | 820-2840 cells/μL | 2360 | 1040 |
| $CD3^+$ T cells | 550-2202 cells/μL | 2066 | 893 |
| $CD4^+$ T cells | 365-1437 cells/μL | 1247 | 628 |
| $CD8^+$ T cells | 80-846 cells/μL | 831 | 236 |
| $CD19^+$ B cells | 45-409 cells/μL | 128 | 32 |
| $CD16^+CD56^+$ natural killer cells | 59-513 cells/μL | 127 | 89 |

**TABLE E3.** The relative distribution of B-cell subsets in the patient and her brother

| B-cell subset | Reference interval | Patient | Brother |
|---|---|---|---|
| $CD19^+$ B cells (% of $CD45^+$ cells) | 2.8%-17.4% (% of $CD45^+$ cells) | 4.5 | 2.9 |
| $CD20^+$ B cells | 3.2%-16.8% (% of $CD45^+$ cells) | 4.7 | 3.2 |
| Total memory B cells | 6.3%-52.8% (% of $CD19^+$ cells) | 29.9 | 57.9 |
| Nonswitched memory B cells | 1.7%-29.3% (% of $CD19^+$ cells) | 15.9 | 23 |
| Switched memory B cells | 2.3%-26.5% (% of $CD19^+$ cells) | 5 | 24.9 |
| Transitional B cells | 1.2%-50.7% (% of $CD19^+$ cells) | 8.2 | 5.8 |
| Plasmablasts | 4.1%-42.2% (% of $CD19^+$ cells) | 12.2 | 2.7 |
| $CD21^+$ B cells | 92.1%-99.6% (% of $CD19^+$ cells) | 94.4 | 94.2 |